Measurement of propagation velocity of bound electromagnetic fields in near zone

A. L. Kholmetskii, O. V. Missevitch, and R. Smirnov-Rueda

Citation: J. Appl. Phys. **102**, 013529 (2007); doi: 10.1063/1.2749415
View online: http://dx.doi.org/10.1063/1.2749415
View Table of Contents: http://jap.aip.org/resource/1/JAPIAU/v102/i1
Published by the American Institute of Physics.

Measurement of propagation velocity of bound electromagnetic fields in near zone

A. L. Kholmetskii
Department of Physics, Belarus State University, 4 Nezavisimosti Avenue, 220030 Minsk, Belarus

O. V. Missevitch
Institute for Nuclear Problems, 11 Bobruiskaya Street, 220030 Minsk, Belarus

R. Smirnov-Rueda[a)]
Applied Mathematics Department, Faculty of Mathematics, Complutense University, 28040 Madrid, Spain

(Received 1 February 2007; accepted 15 May 2007; published online 12 July 2007)

We start with the general approach based on conventional solutions to Maxwell's equations and show that in the near zone of macroscopic electromagnetic sources the electromotive force produced in receiving loop antenna is intimately linked to the fundamental structure as well as to causal properties of the classical electromagnetic field as a superposition of bound and radiation components. As a consequence, we propose and implement a direct experimental procedure for the correct identification of retarded positions of bound field contributions on the oscilloscope time scale as a function of a distance from the emitting loop antenna. It provides unambiguous empirical information on causal characteristics of bound electromagnetic fields. According to the observation of no retardation inside the near zone of the emitting loop antenna, the experimental evidence for nonlocal properties of bound electromagnetic fields is reported. © *2007 American Institute of Physics*. [DOI: 10.1063/1.2749415]

I. INTRODUCTION

Classical electrodynamics is an empirically well supported theory within its domain of application which boundary is established by quantum electrodynamics. The advent of quantum theory has not led to the collapse of classical views but, rather, has helped to highlight their limits of applicability. Moreover, in modern physics there is one basic issue (which has an entirely classical origin) concerning the unique propagation rate of all fundamental physical forces with the speed of light. This basic premise of the classical standpoint seems to be sometimes at odds with the observable behavior of quantum mechanical systems at very small length scales where some indications on nonlocality take place. In spite of the considerable effort to place all quantum mechanical effects into the classical locality (or causality) framework, it is generally acknowledged that there is still no conceptually unproblematic consistent causal approach to observable manifestations of nonlocality within domains of quantum theories.

The notions of locality and causality are central to theorizing in classical electrodynamics and they are assumed to be trustworthy for any *macroscopic* region, at least as large as atomic or molecular length scale, so establishing a natural boundary with quantum effects. However, the actual extrapolation of the causality and locality properties of classical electromagnetic (em) fields to very small distances (up to quantum mechanical limits) has very scarce empirical basis, i.e., it is practically taken for granted without any serious experimental support. In fact, after Hertz's discovery of em waves[1] in agreement with the predictions of Maxwell's theory, the fundamental task in verifying propagation characteristics of classical em fields had been taken as definitively complete. Perhaps, it can be qualified as the main reason for persistent disinterest in providing a solid empirical ground for em field causality properties at very small macroscopic level. As a consequence, since the time of Hertz's experiments all systematic empirical analysis of retardation rates of em fields in space regions very close to em field sources (*near zone*) had been either abandoned or given already little fundamental importance.

However, there are several methodological and historical circumstances[2] as well as recent experimental data[3] that show the obvious necessity to obtain *additional empirical information* in order to endorse or disprove the existent status of causality at very small distances. As it already has been anticipated in Refs. 2 and 3, the actual criteria on experimental verification of em field causality (due to Hertz's experiments) might on the first glance look foundationally unproblematic but it does not take into account the complex structure of the whole em field and the latter is especially relevant at very small distances.

Modern classical electrodynamics[4,5] distinguishes velocity-dependent (bound) and acceleration-dependent (radiation) components. In order to avoid some possible misunderstandings, we remind that bound contributions (known also as induction fields[6,7]) represent dynamic counterpart of static (or quasistatic) fields. In the absence of acceleration there is no radiation and, for instance, electric bound component turns out to represent the Coulomb electric field for a charge at rest (or uniform motion). The ratio of the radiation to bound field strength increases with distances R from the em field source, and the radiation contribution becomes dominant at relatively large distances. In common situations,

[a)]Electronic mail: smirnov@mat.ucm.es

the two contributions are equal at a distance from a source $\lambda/2\pi$ (λ is the wavelength of em radiation). The space domain $R>\lambda/2\pi$ where the radiation predominates is called the *far zone*. The region $R<\lambda/2\pi$ where the bound field predominates is close to the em field source and it is regarded as the near zone.

The clear distinction between both space domains should be taken into account at constructing a consistent and rigorous approach to em field causality at all macroscopic length scales. Nevertheless, available scientific literature shows that among the criteria for evaluating existent empirical tests of causality, the internal structure of em field (superposition of bound and radiation components) does not play any important role. Not distinguishing carefully enough between bound and radiation components is one of the main reasons why the experimental verification of em field propagation (causality) properties cannot be taken as definitively complete.[2,3] Any ideally rigorous test of the causal behavior of the whole em field must be based on separate (or individual) tests for bound and radiation components. Nearly one century of technical treatment of em radiation leaves no doubt with respect to its causal properties at every macroscopic length scales (up to atomic level). On the contrary, due to the lack of any detailed information on causal characteristics of bound em fields, the motivation now is to complete this task experimenting with em field within the near zone.

Thus, at uhf frequency ~125 MHz, the boundary $\lambda/2\pi$ between the two domains is placed approximately at 40 cm from the em field source. Laboratory measurements[3] were carried out at this frequency within the macroscopic region (40–200 cm) where the ratio of the bound to radiation field strength was not too far from unity. At larger distances the em radiation predominates, and in our experiments it constituted nearly the whole signal detected at 300 cm. We used this information in order to reconstruct radiation components at different positions within the region of space of 40–200 cm. Then, we could compare it with the whole em signal (superposition of bound and radiation components) detected at the same spatial points. Thus, the time difference between the detectable signal and radiation component became available from the experiment and could be studied as a function of a distance between emitting and receiving antennas. This approach to bound fields has been regarded as *zero-crossing method*.[3] Interestingly, experimental data showed a considerable disagreement with theoretical predictions for the case when the standard causality properties are supposed to be applicable both to bound and radiation fields. Moreover, experimental data nearly perfectly fitted the prediction calculated numerically for the case when the propagation rate of bound fields in near zone highly exceeds the velocity of light. Importantly, these observations have to be demarcated from theoretical results on retardation characteristics exhibited by scalar and vector potentials in a particular gauge, since em fields are independent from the gauge choice in displaying experimentally verifiable properties of causality and propagation.[8–10]

There is, then, a perspective open for a possible disagreement between the actual status of causality (or locality) and observable behavior of bound fields in the near zone. Nevertheless, the zero-crossing method alone suggested and implemented in Ref. 3 is obviously insufficient for arriving at trustworthy quantitative conclusions since it is based on the analysis of some specific time moment at which the total composite signal (bound plus radiation terms) crosses the zero level. As a result, it can be sensitive only to a notable difference between propagation characteristics of bound and radiation field components in the near zone without providing exact values of the propagation rate of bound em fields and its possible dependence on a distance from the emitting source. This intrinsic limitation of the zero-crossing method suggests a search of an alternative and independent approach in which experimental observation of the causal propagation of bound em fields might be considerably amended. Following this suggestion of improvement as a step forward in comparison with the zero-crossing method, we propose in this work to study bound field components separately by explicit decomposition of the detectable signal on bound and radiation contributions within the whole time interval. To fulfill this task it will involve a consideration of an additional coaxial configuration between emitting and receiving antennas as well as an extension of the theoretical description given in Ref. 3. The use of the experimental setup implemented already in the preceding work[3] will ensure an important possibility of cross verification and qualitative comparison of new experimental data with the previous results.

II. THEORETICAL BACKGROUND

A. em field structure

The general approach to magnetic field structure as a superposition of bound (velocity-dependent) $\mathbf{B_u}$ and radiation (acceleration-dependent) $\mathbf{B_a}$ components generated by em field source (time-varying current) as well as to the actual account of retardation effects is explicable in terms of the time-varying Biot-Savart's law,[7,11]

$$\mathbf{B}(\mathbf{R},t)=\mathbf{B_u}+\mathbf{B_a}=\frac{1}{4\pi\varepsilon_0 c^2}\times\int\left[\frac{(\mathbf{J})_c}{R'^3}+\frac{1}{cR'^2}\left(\frac{\partial\mathbf{J}}{\partial t}\right)_c\right]\times\mathbf{R}'dV_s, \tag{1}$$

where $\mathbf{J}$ is the conduction current density, $\mathbf{R}$ is a position vector of a point of observation, R' is the distance between the point of observation and the source point where the volume element of integration dV_s is located, and the corresponding quantity placed inside the parentheses is being determined at the retarded time $t-R'/c$.

We recall that Eq. (1) is considered exact in the so-called *low velocity relativistic limit*,[7,11] which implies negligible *the ratio* of velocities of conduction charges to the speed of light, while retardation effects are still taken into account. For filamentary currents (in particular, for thin wire loops that are under study in this work) an expression analogous to Eq. (1) can be obtained in the form of a line integral if the centripetal acceleration of conduction charges is neglected in comparison with their linear acceleration,[11]

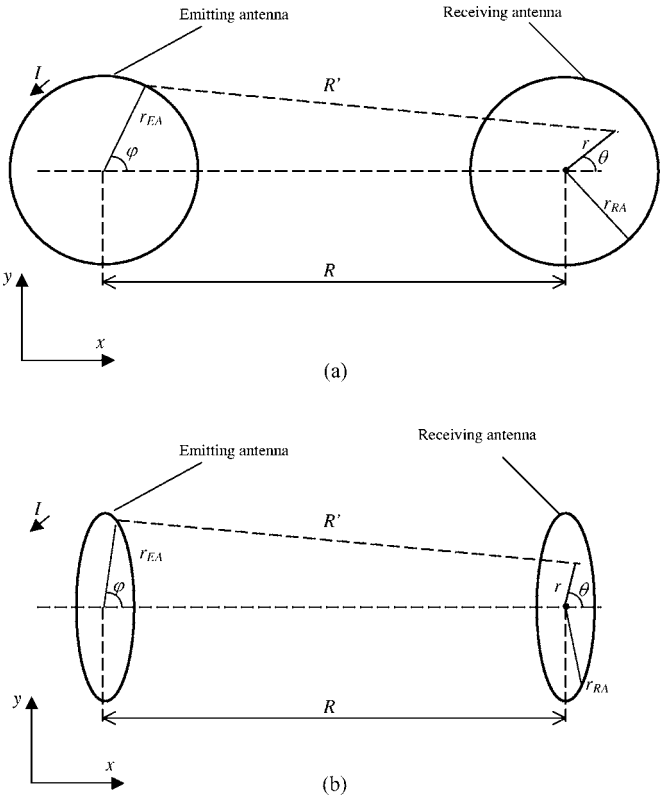

FIG. 1. Positional configuration between the emitting and receiving antennas: (a) coplanar configuration and (b) coaxial configuration.

$$\mathbf{B} = \mathbf{B_u} + \mathbf{B_a} = \frac{1}{4\pi\varepsilon_0 c^2}\oint_\Gamma \left[\frac{(I)_c}{R'^2} + \frac{1}{cR'}\left(\frac{\partial I}{\partial t}\right)_c\right]\mathbf{k}\times\mathbf{n}dl, \tag{2}$$

where $\mathbf{n}=\mathbf{R}'/R'$, I is the conduction current, $\mathbf{k}$ is the unit vector in the direction of $\mathbf{I}$, i.e., $\mathbf{I}=I\mathbf{k}$, and dl is an infinitesimal element of the loop line Γ.

Retarded integrals (1) and (2) describe causal relations between em phenomena taking place in emitting loop antenna (EA) and present-time value of magnetic field that is closely associated with the actual understanding of the causality principle.

B. Electromotive force structure

In this sense, *electromotive force* (emf) $\varepsilon(t)$ induced in receiving loop antenna (RA) is also understood as a retarded cause-effect relationship described by Faraday's induction law,

$$\varepsilon(t) = -\frac{1}{4\pi\varepsilon_0 c^2}\frac{d}{dt} \times \int\int_S \left\{\oint_\Gamma \left[\frac{(I)_c}{R'^2} + \frac{1}{cR'}\left(\frac{\partial I}{\partial t}\right)_c\right]\mathbf{k}\times\mathbf{n}dl\right\}d\mathbf{S}, \tag{3}$$

where S is the area of RA.

Further on we shall consider two particular positional configurations between EA and RA (see Fig. 1). *Coplanar* configuration [Fig. 1(a)] will take place if both EA and RA loops belong to the same plane. By analogy, *coaxial* configuration [Fig. 1(b)] will correspond to the positions of EA and RA sharing the same axis of symmetry. As a result, Eq. (3) can be rewritten in a more convenient form,

$$\varepsilon = \frac{1}{4\pi\varepsilon_0 c^2}\int_0^{r_{RA}}\int_0^{2\pi}\int_0^{2\pi}\left[\frac{(\partial I/\partial t)_c}{R'^3} + \frac{(\partial^2 I/\partial t^2)_c}{cR'^2}\right] \times \xi r_{EA}^2 r dr d\theta d\varphi, \tag{4}$$

where R' and ξ depend on the positional configuration between EA and RA as

$$R'_{pl} = [(R - r_{EA}\cos\varphi + r\cos\theta)^2 + (r_{EA}\sin\varphi - r\sin\theta)^2]^{1/2}, \tag{5}$$

$$R'_{ax} = [R^2 + (r_{EA}\cos\varphi - r\cos\theta)^2 + (r_{EA}\sin\varphi - r\sin\theta)^2]^{1/2}, \tag{6}$$

$$\xi_{pl} = \left[1 - \frac{r}{r_{EA}}\cos(\theta-\varphi) - \frac{R\cos\varphi}{r_{EA}}\right], \tag{7}$$

$$\xi_{ax} = \left[1 - \frac{r}{r_{EA}}\cos(\theta-\varphi)\right], \tag{8}$$

where we denote coplanar or coaxial configuration by subindex pl or ax, respectively; all other notations can be found in Fig. 1.

Mathematical treatment of retarded integrals frequently requires consideration of verisimilar approximations. The most commonly used one is the so-called *electrically small antenna*. In the framework of this requirement the radii r_{EA} and r_{RA} of EA and RA loops are to be small enough in comparison with the em radiation wavelength $\lambda \gg r_{EA}$, r_{RA}. The other frequently used precondition is *quasistationary current approximation*, which means that the conduction current I has the same phase in all angular coordinates φ of EA at some present time t, i.e., $I(t,\varphi)=I(t)f(\varphi)$. In particular, we shall use one special case of quasistationary current approximation when $f(\varphi)$ does not depend on φ. Finally, in order to use a series expansion with respect to r_{EA}/R and r_{RA}/R, we shall restrict our analysis of em fields to distances $R > r_{EA}$, r_{RA}.

If the time variation of $I(t)$ is close to harmonic (quasiharmonic approximation will be fulfilled in our experimental realization), all higher order time derivatives $\partial I/\partial t$, $\partial^2 I/\partial t^2$, etc., also will not depend on φ and then will have the same present-time value over the perimeter of the emitting loop. Hence one can factor $\partial I/\partial t$, $\partial^2 I/\partial t^2$, etc., out from the integral sign and neglecting second order retardation effects, Eq. (4) can be presented in a general compact format which will be convenient for further considerations (readers interested in full derivation can refer to Appendix A),

$$\varepsilon = -\frac{S_{EA}S_{RA}}{4\pi\varepsilon_0 c^2}\left[k_{b1}\frac{(\partial I/\partial t)_c}{R^3} + k_{b2}\frac{(\partial^2 I/\partial t^2)_c}{cR^2} + k_{f1}\frac{(\partial^2 I/\partial t^2)_c}{cR^2} + k_{f2}\frac{(\partial^3 I/\partial t^3)_c}{c^2 R}\right], \tag{9}$$

where

$$k_{b1} = \frac{R^3}{\pi^2 r_{\mathrm{RA}}^2} \int_0^{r_{\mathrm{RA}}} \int_0^{2\pi} \int_0^{2\pi} \frac{\xi}{R'^3} r dr d\theta d\varphi, \tag{10}$$

$$k_{b2} = \frac{R^2}{\pi^2 r_{\mathrm{RA}}^2} \int_0^{r_{\mathrm{RA}}} \int_0^{2\pi} \int_0^{2\pi} (R - R') \frac{\xi}{R'^3} r dr d\theta d\varphi, \tag{11}$$

$$k_{f1} = \frac{R^2}{\pi^2 r_{\mathrm{RA}}^2} \int_0^{r_{\mathrm{RA}}} \int_0^{2\pi} \int_0^{2\pi} \frac{\xi}{R'^2} r dr d\theta d\varphi, \tag{12}$$

$$k_{f2} = -\frac{R}{\pi^2 r_{\mathrm{RA}}^2} \int_0^{r_{\mathrm{RA}}} \int_0^{2\pi} \int_0^{2\pi} (R - R') \frac{\xi}{R'^2} r dr d\theta d\varphi, \tag{13}$$

and $S_{\mathrm{EA}} = \pi r_{\mathrm{EA}}^2$ and $S_{\mathrm{RA}} = \pi r_{\mathrm{RA}}^2$.

The advantage in having a structured expression (9) is that one can easily follow the specific origin of every contribution (either due to *bound* or to *free radiation* magnetic fields), obtaining necessary insight into the underlying structure of the resultant emf induced in RA. Thus, according to the analysis effected in Appendix A, the reader can check that the first two terms proportional to dimensionless coefficients k_{b1} and k_{b2} are originated by bound (or velocity-dependent) magnetic fields, whereas the last two terms are due to free radiation (or acceleration-dependent) components.

In order for Eq. (9) to be suitable for practical implementations, dimensionless coefficients [(10)–(13)] are to be evaluated in every particular configuration between EA and RA as a function on a distance R. It is easy to show that coefficients [(10)–(13)] take definite numerical values at large distances when $R \gg r_{\mathrm{EA}}, r_{\mathrm{RA}}$. In fact, for coplanar configuration $k_{b1}^{\mathrm{pl}} = k_{b2}^{\mathrm{pl}} = k_{f2}^{\mathrm{pl}} = 1$ and $k_{f1}^{\mathrm{pl}} = 0$ in zero order approximation with respect to ratios r_{EA}/R and r_{RA}/R, as it already had been shown in Refs. 7, 12, and 3. In coaxial configuration, coefficients [(10)–(13)] take already definite numerical values $k_{b2}^{\mathrm{ax}} = k_{f2}^{\mathrm{ax}} = 0$ and $k_{b1}^{\mathrm{ax}} = k_{f1}^{\mathrm{ax}} = 2$ in first order approximation with respect to ratios r_{EA}/R and r_{RA}/R. It means that at large distances $R \gg r_{\mathrm{EA}}$ Eq. (9) can be substituted by equivalent expressions with a smaller number of terms.

Thus, the use of (9) for finding the emf in RA can be restricted by taking into account only zero and first order terms with respect to ratios r_{EA}/R and r_{RA}/R. Neglecting second order terms $\sim (r_{\mathrm{EA}}/R)^2$ and $(r_{\mathrm{RA}}/R)^2$ in evaluation of (10)–(13), one can find that $k_{f1} = 0$ in coplanar configuration so that

$$\varepsilon_{\mathrm{pl}} = -\frac{S_{\mathrm{EA}} S_{\mathrm{RA}}}{4\pi\varepsilon_0 c^2} \left[k_{b1}^{\mathrm{pl}} \frac{(\partial I/\partial t)_c}{R^3} + k_{b2}^{\mathrm{pl}} \frac{(\partial^2 I/\partial t^2)_c}{cR^2} + k_{f2}^{\mathrm{pl}} \frac{(\partial^3 I/\partial t^3)_c}{c^2 R} \right], \tag{14}$$

where $k_{b1}^{\mathrm{pl}} = k_{b2}^{\mathrm{pl}} = k_{f2}^{\mathrm{pl}} = 1$ if $(r_{\mathrm{EA}}/R), (r_{\mathrm{RA}}/R) \ll 1$.

Conversely, due to the proper symmetry of coaxial configuration coefficients $k_{b2}^{\mathrm{ax}} = k_{f2}^{\mathrm{ax}} = 0$ and $k_{b1}^{\mathrm{ax}} = k_{f1}^{\mathrm{ax}} = 2$ in first order approximation with respect to ratios r_{EA}/R and r_{RA}/R,

$$\varepsilon_{\mathrm{ax}} = -\frac{2 S_{\mathrm{EA}} S_{\mathrm{RA}}}{4\pi\varepsilon_0 c^2} \left[\frac{(\partial I/\partial t)_c}{R^3} + \frac{(\partial^2 I/\partial t^2)_c}{cR^2} \right]. \tag{15}$$

Therefore, if we take $r_{\mathrm{RA}} = r_{\mathrm{EA}} = 5$ cm that is equal to the radii of EA and RA implemented in our experimental setup, numerical calculations based on (15) will not produce more than 5% deviation from the emf evaluated using exact expression (4) within the space domain $R \geqslant 20$ cm. For coplanar configuration, a numerical comparison between (4) and (14) provided the condition $R \geqslant 40$ cm when the requirement on 5% admissible deviation error is fulfilled. As a result, one can see that in coaxial configuration the use of (15) at smaller distances requires weaker restrictions in comparison with those for (14) in coplanar configuration.

The coaxial configuration has another important advantage over the coplanar configuration in providing the resultant emf as a superposition of only R^{-3} and R^{-2} terms, whereas the R^{-1} term as part of em radiation turns out to be fully suppressed. It conforms to the well-known fact that there is no magnetic dipole radiation along the axis of symmetry of EA.

In view of the further needs of signal processing, we present (14) and (15) in a more practical form by normalizing $\varepsilon_{\mathrm{pl}}$ and $\varepsilon_{\mathrm{ax}}$ by factors $(-S_{\mathrm{EA}} S_{\mathrm{RA}}/4\pi\varepsilon_0 c^2)$ and $(-2 S_{\mathrm{EA}} S_{\mathrm{RA}}/4\pi\varepsilon_0 c^2)$, respectively,

$$\tilde{\varepsilon}_{\mathrm{pl}} = \frac{k_{b1}^{\mathrm{pl}}}{R^3} \left(\frac{\partial I}{\partial t} \right)_c + \frac{k_{b2}^{\mathrm{pl}}}{cR^2} \left(\frac{\partial^2 I}{\partial t^2} \right)_c + \frac{k_{f2}^{\mathrm{pl}}}{c^2 R} \left(\frac{\partial^3 I}{\partial t^3} \right)_c, \tag{16}$$

$$\tilde{\varepsilon}_{\mathrm{ax}} = \frac{1}{R^3} \left(\frac{\partial I}{\partial t} \right)_c + \frac{1}{cR^2} \left(\frac{\partial^2 I}{\partial t^2} \right)_c, \tag{17}$$

where $\tilde{\varepsilon}_{\mathrm{pl}} = -\varepsilon_{\mathrm{pl}}/(S_{\mathrm{EA}} S_{\mathrm{RA}}/4\pi\varepsilon_0 c^2)$, $\tilde{\varepsilon}_{\mathrm{ax}} = -\varepsilon_{\mathrm{ax}}/(2 S_{\mathrm{EA}} S_{\mathrm{RA}}/4\pi\varepsilon_0 c^2)$, and coefficients k_{b1}^{pl}, k_{b2}^{pl}, and k_{f2}^{pl} are determined by Eqs. (10)–(13) and depend on R, r_{EA}, and r_{RA}.

To conclude our discussion of the standard approach, we note that expressions (14) and (15) [or (16) and (17)] for predicting the time variation of emf in RA are in agreement with the principle of finite causal propagation at universal speed of light by attaching the same retardation rate to both bound and free radiation magnetic fields. Therefore, it can be taken as the basis for theoretical predictions to be compared with experimental observations at all length scales. If causal conditions meaningful for bound and radiation fields are distinct, then one would expect to detect observable deviations from theoretical predictions based on (16) and (17).

One can also use an obvious advantage of the coaxial configuration in which the resultant emf (17) is composed only of R^{-3} and R^{-2} terms due to bound and radiation contributions, respectively. Moreover, two different contributions can be studied separately within the space regions where they are dominant. In fact, at larger distances $(R > \lambda/2\pi)$ the R^{-2} radiation contribution and at smaller distances $(R < \lambda/2\pi)$ the R^{-3} bound contribution will impose the retardation rate and the dependence on a distance R of the whole signal. It provides the basis for a methodologically rigorous approach to bound fields in the near zone of em sources.

C. Methodological approach to causal properties of bound magnetic fields

Here it is worth reminding that there is actually no explicit empirical information on bound fields as far as their propagation properties are concerned. In view of experimental indications[3] on a possible inadequacy of standard views in the near zone, it would be reasonable to theoretically explore the type of alternative predictions when the velocity of propagation of bound fields (further denoted as v) can differ from the speed of light. Thus, if one discerns v from c and follows the procedure described in Appendix A for a rigorous account of retardation effects, one can check that the fundamental structure of the resultant emf as a superposition of bound and radiation contributions remains unalterable. Moreover, dimensionless coefficients [(10)–(13)] due to a particular configuration between EA and RA keep also unchanged,

$$\tilde{\varepsilon}_{\mathrm{pl}} = \frac{k_{b1}^{\mathrm{pl}}}{R^3}\left(\frac{\partial I}{\partial t}\right)_v + \frac{c}{v}\frac{k_{b2}^{\mathrm{pl}}}{cR^2}\left(\frac{\partial^2 I}{\partial t^2}\right)_v + \frac{k_{f2}^{\mathrm{pl}}}{c^2 R}\left(\frac{\partial^3 I}{\partial t^3}\right)_c \tag{18}$$

and

$$\tilde{\varepsilon}_{\mathrm{ax}} = \frac{1}{R^3}\left(\frac{\partial I}{\partial t}\right)_v + \frac{1}{cR^2}\left(\frac{\partial^2 I}{\partial t^2}\right)_c, \tag{19}$$

where quantities $(\partial I/\partial t)_v$ and $(\partial^2 I/\partial t^2)_v$ are being determined at the retarded time $t-R/v$.

Equations (18) and (19) are model dependent and can be regarded as methodological analogies of standard Eqs. (16) and (17), sharing the same theoretical predictions either at $v=c$ or at very large distances $R \gg \lambda/2\pi$, where the R^{-3} contribution becomes irrelevant. Thus, the use of model Eqs. (18) and (19) can be justified only if there are clear experimental evidences for the inadequacy of Eqs. (16) and (17) to describe empirical data within a finite region of space referred to as the near zone where bound fields are dominant. In fact, according to mathematical properties of (18) and (19), the whole signal $\tilde{\varepsilon}_{\mathrm{pl}}$ or $\tilde{\varepsilon}_{\mathrm{ax}}$ is the most sensitive to a possible difference between v and c only in the near zone of em sources. It reflects the general assumption that bound and free radiation fields are independent of each other in the corresponding area of their domain. Thus, within the near zone the R^{-3} contribution prevails and determines propagation characteristics of the whole signal that can be studied experimentally in order to obtain convincing evidence in favor of either $v=c$ or $v \neq c$. An appropriate experimental procedure will be defined in the next section. However, before doing it we shall describe a particular experimental setup and technical characteristics of EA and RA used to produce $\varepsilon_{\mathrm{pl}}$ and $\varepsilon_{\mathrm{ax}}$ in coplanar and coaxial configurations, respectively.

III. EXPERIMENTAL MEASUREMENTS AND DATA PROCESSING

Figure 2 shows a diagram of the EA circuit which the driving element is constituted by a fast high-voltage (HV) spark gap (SG) connected to the antenna via the blocking capacitor C. In order to drastically reduce the absolute value of electric dipole radiation and to reach the requirements imposed by quasistationary current approximation, both EA and RA were divided into sections, as it is shown in Fig. 3. Technical characteristics of multisection antennas correspond to the experimental setup described and used in our previous work.[3] Quasiharmonic current pulse was derived from ~5.5 kV spark gap, and its estimated period was approximately 8 ns that conforms to $\lambda \sim 2.5$ m wavelength of em radiation. Following modern standards of the antenna metrology techniques, we used the pulsed mode generation of em signals to avoid the reflected wave interference. Besides, it allowed us to achieve a considerable peak amplitude of em field strength at low average power consumption. Antenna radii $(r_{\mathrm{EA}}, r_{\mathrm{RA}})$ and widths $(h_{\mathrm{EA}}, h_{\mathrm{RA}})$ were equal to 5 cm keeping in line with adopted approximations.

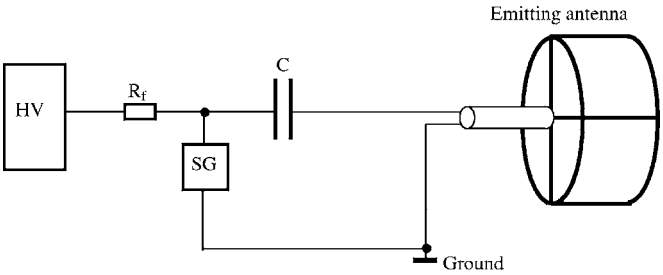

FIG. 2. Technical realization of the emitting antenna (EA) driving circuit.

To perform our measurements we set EA and RA either in coplanar [Fig. 1(a)] or in coaxial [Fig. 1(b)] configuration and keeping their orientations unchanged, we varied the distance R between their centers. In coaxial configuration the range of variation of R was 20–300 cm, whereas in coplanar position it was $R=40$–300 cm. For the region of space $R \leqslant 100$ cm we used a small step $\Delta R=10$ cm, and for larger distances $R>100$ cm the step was doubled in size $\Delta R=20$ cm. At each space position emf signal $\varepsilon(t)$ induced in

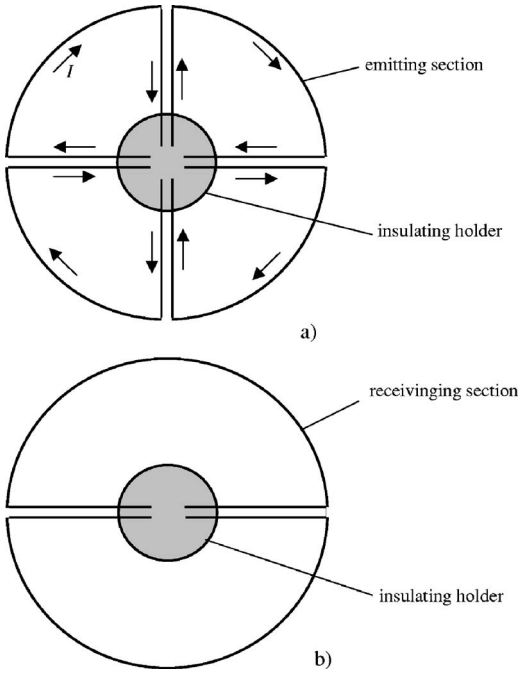

FIG. 3. (a) The emitting antenna (EA) cross section (the arrows show the direction of the conduction current in all sections). (b) The receiving antenna (RA) cross section.

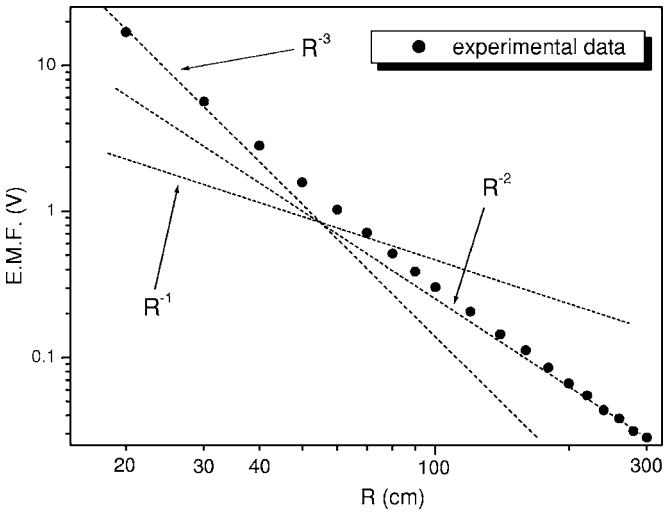

FIG. 4. Coaxial configuration: the amplitude of the recorded emf produced in RA as a function of a distance R.

RA was recorded in a digital format with the oscilloscope Tektronix TDS-3052. Its sampling rate is 5 G sample/s or 0.2 ns/channel and expected time resolution is about 0.02 ns. The maximal voltage sensitivity available by the oscilloscope is 1 mV/division.

Both EA and RA were mounted on a wooden table removing all metallic objects (with the capacity to reflect em radiation) at distances exceeding 1.5 m in all ranges of variation of R. It assured no measurement interference by reflected em waves during the period of the first 8 ns. Each signal was recorded after 128 averaging and numerically interpolated by cubic splines. It allowed us a quantitative comparison with theoretical predictions based on (16) and (17).

A. Processing of signals in coaxial configuration

Our first intention was to verify the two-component structure (R^{-3} and R^{-2} terms) of the whole signal predicted by the standard Eq. (17) and its methodological analogy in the form of Eq. (19). Starting with $R=20$ cm we measured $\varepsilon_{\max}(R)$ (the maximum amplitude of a signal as a function on a distance) for $R=20-300$ cm. The result is plotted in Fig. 4 in logarithmic scales. The slope of black circles, that are meant to represent the measurements, was found to be approaching -3 at small distances (near zone), whereas at larger distances one can clearly see the tendency of the slope to change its value and eventually it tends to -2 in far zone. In the whole range of variation of R the slope of the empirical curve does not reach values close to -1, indicating a negligibly small contribution of possible radiation components proportional to R^{-1} and, therefore, confirming that that two-component analysis of detectable signals in coaxial configuration is actually realistic.

The next task is to approach a decomposition of recorded signals on R^{-3} bound and R^{-2} radiation contributions within a wide range of variation of $R=20-240$ cm. The amplitude and retardation phase relationships of each term in the resultant emf are clearly specified by the standard Eq. (17). The free radiation contribution $\varepsilon_f(t,R)$ proportional to R^{-2} is dominant at large distances $R_{\max} \gg \lambda/2\pi$ and, therefore, constitutes nearly the whole signal $\varepsilon_f(t,R_{\max}) \cong \varepsilon(t,R_{\max})$. Once the signal has been recorded at $R_{\max}$ and taking into account that radiation fields propagate with the speed of light, one can reconstruct the radiation contribution $\varepsilon_f(t,R)$ as a part of the whole signal $\varepsilon(t,R)$ at each position within the space domain $R=20-240$ cm. It can be implemented by a simple rescaling of $\varepsilon(t,R_{\max})$ with the factor $(R_{\max}/R)^2$ as well as by corresponding time shift $(R_{\max}-R)/c$. Then, according to the standard Eq. (17), the bound contribution $\varepsilon_b(t,R)$ has to be recovered at each spatial position by subtraction of the reconstructed radiation signal $\varepsilon_f(t,R)$ from the recorded signal $\varepsilon(t,R)$ (readers interested in the rigorous formalization of this procedure can refer to the first part of the Appendix B), position of bound contributions obtained as a function of R is equivalent to the knowledge of corresponding time shifts $\Delta t_b(R_1,R_2)$ between bound contributions detected at different distances R_1 and R_2. Then the average propagation velocity of bound fields as a function of a distance R can be evaluated by $\bar{v}[(R_2+R_1)/2]=(R_2-R_1)/\Delta t_b(R_1,R_2)$, where R_1 and R_2 is a pair of the closest spatial positions so that $R_2-R_1=\Delta R$ is the step used in our measurements.

We took $R_{\max}=300$ cm and at this distance the radiation contribution constituted nearly 90% of the whole recorded signal $\varepsilon(t,R_{\max})$, defining thus the precision of the above-described one-step decomposition. As a first approximation, it is already acceptable to estimate the retardation rate of the bound component at different R. Within the limit of precision available in our measurements, we reconstructed the position of bound contributions inside the near zone and did not find any observable retardation which was expected on the base of the standard Eq. (17). In order to improve the precision of the one-step decomposition, we performed an additional iteration procedure described in the second part of Appendix B. There we define a numerical method which uses small variations of $\Delta t_b(R_1,R_2)$ as a fitting parameter between the experimentally obtained data and Eq. (19). Here we stress that the model Eq. (19) (where v is unknown and to be determined from experimental data) was used only after having obtained a strong disagreement with the expected retardation rate for bound em fields within the near zone of the EA predicted by the standard Eq. (17).

Results of iteration procedure are presented in Fig. 5 and show a separation of the recorded signal into the R^{-3} bound and the R^{-2} radiation contributions. As in the case of one-step decomposition we again observed no retardation of bound components between $R=20$, 30, and 40 cm. There are also clear indications on the absence of retardation of bound fields within the initial domain $R=0-20$ cm. Set in other terms, bound fields appear to possess a propagation velocity highly exceeding the speed of light inside the near zone $R \leqslant \lambda/2\pi \simeq 40$ cm. It turns out to be in line with the results of our previous work.[3]

At larger distances, we observed finite time shifts Δt_b that are still considerably smaller than $\Delta t=\Delta R/c$ expected for the standard retardation rate of R^{-3} contributions. Between $R=40$ and 50 cm the time shift Δt_b corresponded to the average value $v=8.2c$, whereas between $R=50$ and 60 cm Δt_b gave $v=4.3c$. Nevertheless, at larger distances the

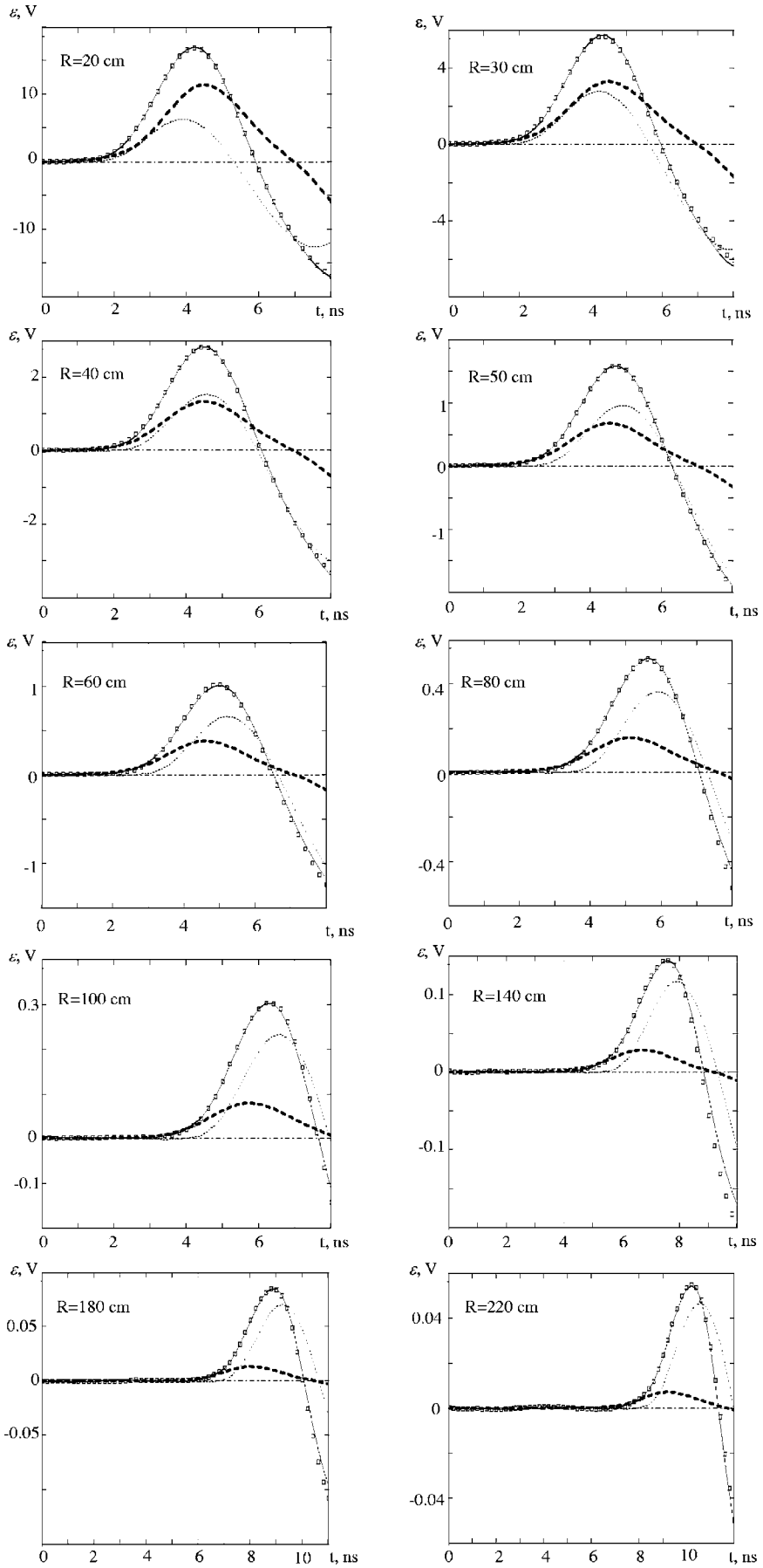

FIG. 5. Coaxial configuration: visualization of the detectable signal produced in the RA at different spatial positions; all subplots show the result of the decomposition of the recorded signal (hollow squares) into R^{-3} bound (dash lines) and R^{-2} radiation (dot lines) contributions. Continuous line is a superposition of R^{-3} and R^{-2} components obtained in the decomposition procedure.

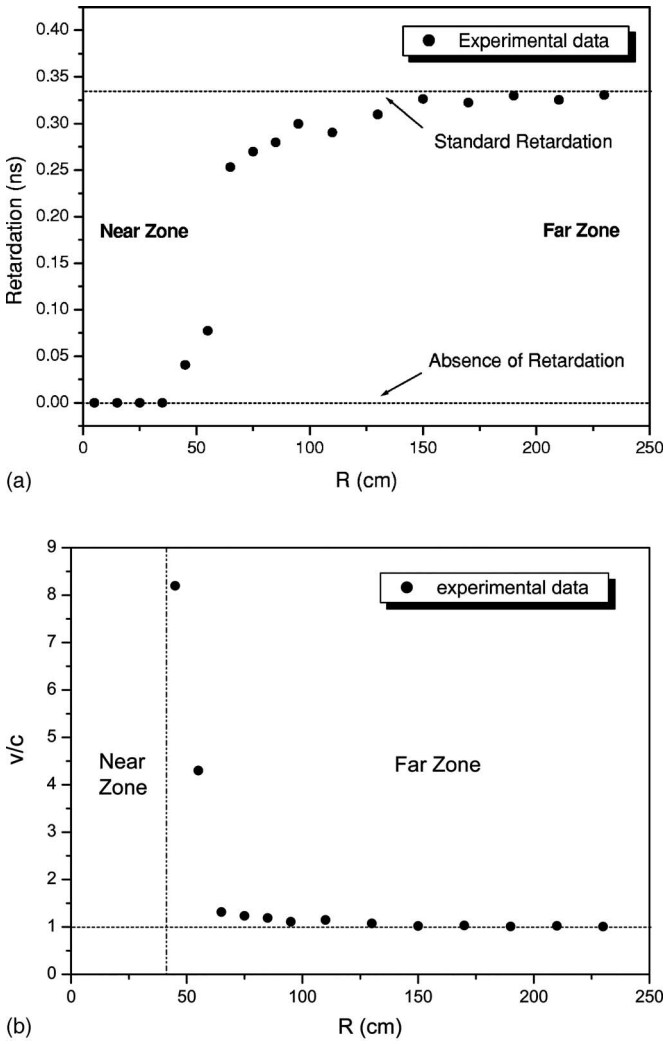

FIG. 6. (a) Retardation time shift $\Delta t_b(R)$ of bound contribution measured between two closest spatial positions. At large distances the retardation time shift tends to the standard value $\Delta t = 10\ \mathrm{cm}/c \simeq 0.33$ ns. (b) The propagation velocity of bound fields determined as reciprocal to $\Delta t_b(R)$ dependence.

observed time shift tended to the value $\Delta t = 10\ \mathrm{cm}/c \cong 0.33$ ns which is assumed if the speed of light c determines the retardation. Both dependencies of $\Delta t_b(R)$ and $v(R)$ as functions on a distance can be found in Figs. 6(a) and 6(b), respectively. One clearly notes two strong tendencies of empirical results presented in Fig. 6(a): (a) zero time shifts within the near zone and (b) the approximation to the standard time shift at larger distances. Both of them can be taken as being physically meaningful having in mind that inside, respectively, the near and far zones for the R^{-3} and R^{-2} contributions prevail and determine the propagation rate of the whole signal. However, the type of transition (between both tendencies in Fig. 6) from small to large distances can be qualified as model dependent since it is determined by the methodological Eq. (19)

Here it is also important to emphasize that the value of v is the result of the minimization of the error functional $[R, \Delta t_b(R)]$ [see Eq. (B10)] in Appendix B, which gives a numerical measure of the average deviation between the recorded signal and its theoretical counterpart reproduced on the basis of Eq. (19). To appreciate it we used the same iteration procedure fixing the parameter $v=c$ and calculating the error functional $\delta(R)_{v=c}$. Table I lists the numerical results of both $\delta(R)_{v=c}$ and $\delta[R, \Delta t_b(R)]$, where $\Delta t_b(R)$ undergoes small variations in order to achieve a better fitting. In the latter case the value of the error functional was one order of magnitude smaller than for $v=c$. These results are obviously not in line with expectations based on the assumption of standard causality for bound fields in the near zone of em sources.

TABLE I. Coaxial configuration: comparison of the value of the error functional $\delta(R)_{v=c}$ for the standard assumption $v=c$ and $\delta[R, \Delta t_b(R)]$ for the optimization fitting.

R	$\delta(R)_{v=c}$ (%)	$\delta[R, \Delta t_b(R)]$ (%)
30	1.7	0.26
40	2.6	0.27
50	3.9	0.40
60	3.6	0.35
70	4.3	0.21
80	4.2	0.16
90	4.3	0.16
100	3.5	0.29
120	3.8	0.34
140	3.8	0.28
160	4.3	0.28
180	3.9	0.11
200	3.8	0.24

B. Processing of signals in coplanar configuration

Contrarily to the previous considerations, in coplanar configuration a decomposition of emf into three independent components (one of them with the weight coefficient c/v) according to Eq. (16) or (18) cannot be performed by implementing the iteration procedure of Appendix B. Nevertheless, the explicit form of functions $\partial I/\partial t$ and $\partial^2 I/\partial t^2$ are numerically available already from the previous two-component analysis in coaxial configuration. Since at large distances em radiation predominates, the lacking information on $\partial^3 I/\partial t^3$, which is responsible for the shape of R^{-1} radiation components, can be extracted directly from experimental measurements by recording the detectable signal at $R_{\max} = 300$ cm. Having obtained the shapes of $\partial I/\partial t$, $\partial^2 I/\partial t^2$, and $\partial^3 I/\partial t^3$ and interpolating them with cubic splines, we are in a position to numerically reconstruct the whole signal according to the general analytical expression (18), including the case $v=c$. This is also possible due to the fact that dimensionless coefficients k_{b1}^{pl}, k_{b2}^{pl}, and k_{f2}^{pl} are not dependent on any particular propagation velocity of bound fields.

After having used (10)–(13) to calculate exact numerical values of $k_{b1}^{\mathrm{pl}}(R)$, $k_{b2}^{\mathrm{pl}}(R)$, and $k_{f2}^{\mathrm{pl}}(R)$ as functions of a distance R we are in a position to get a quantitative comparison between numerically synthesized and recorded signals. In our analysis we decided to calculate the value of the error functional $\sigma(R)$,

TABLE II. Coplanar configuration: comparison of the value of the error functional $\sigma(R)$ for the standard causal assumption $v=c$ (the first hypothesis) and the causal framework determined by Eq. (18) as well as by $v(R)$ dependence given in Fig. 6(b) (the second hypothesis).

R	$\sigma(v=c)$ (%)	$\sigma[v(R)]$ (%)
40	12.4	0.89
50	15.3	0.53
60	14.0	0.73
70	7.9	0.58
80	8.5	0.74
90	9.8	0.60
100	8.4	0.67
120	8.8	0.43
140	8.2	0.41
160	7.6	0.46
180	9.6	0.67
200	8.1	0.26

$$\sigma(R) = \frac{100\%}{A(m_2 - m_1)} \sqrt{\sum_{i=m_1}^{m_2} [\varepsilon(R,t_i) - \varepsilon_{\mathrm{syn}}(R,t_i)]^2}, \qquad (20)$$

where $\varepsilon(R,t_i)$ and $\varepsilon_{\mathrm{syn}}(R,t_i)$ are the recorded and synthesized signals in the ith channel on the time scale of the digital oscilloscope, respectively, t_i is the present-time correspondent to the ith channel, A is the amplitude of the recorded signal at the first half-period, and m_1 and m_2 determine the initial and the final channels of the signal half-period, respectively.

Table II refers to the value of $\sigma(R)$ with respect to two basic hypotheses [used to theoretically reconstruct the whole signal $\varepsilon_{\mathrm{syn}}(R,t)$] that are listed below.

(1) Standard retardation condition $v=c$ or Eq. (16).
(2) Causal framework of bound fields is determined by Eq. (18) and by $v(R)$ dependence given in Fig. 6(b).

For the second hypothesis the estimated deviation from the recorded signal turned out to be more than one order of magnitude smaller than that calculated in the case of the standard condition $v=c$. The difference can be visually appreciated in Fig. 7 and numerically in Table II. Importantly, the amplitude of the signal synthesized under the first hypothesis ($v=c$) is notably bigger than the corresponding amplitude of the recorded signal. This circumstance is due to the contribution of the second term in Eq. (16). Contrarily, if the hypothesis 2 is assumed to be valid then the second term in Eq. (18) is fully suppressed at small distances ($R < \lambda/2\pi$) since it is weighted by negligibly small numerical factor c/v in agreement with Fig. 6(b). It gives an additional indication on the propagation velocity of bound fields v highly exceeding the velocity of light in the near zone of em sources by supporting the fact that R^{-2} contribution in coplanar configuration is suppressed at $R < \lambda/2\pi$.

IV. CONCLUSIONS

In order to provide a solid theoretical basis for experimental verification of em field causality in the near zone of macroscopic em sources, we started with the general approach based on conventional solutions to Maxwell's equations. Under electrically small antenna and quasistationary current approximations we derived the general expression (9) for the resultant emf induced in RA specifying the origin of every contribution. In our laboratory measurements we used coplanar and coaxial configurations between EA and RA. In both cases, at relatively large distances $R \gg r_{\mathrm{EA}}$. Eq. (9) has special approximations in the form of Eqs. (14) and (15) providing to the detectable signal a simpler representation as a superposition of a reduced number of components.

In fact, the coaxial configuration has an important advantage in giving the resultant emf as a superposition of only R^{-3} and R^{-2} terms due to bound and radiation contributions, respectively. This circumstance and the well-established fact that radiation fields propagate with the speed of light at any macroscopic length scales assured a direct and unambiguous decomposition of the detectable emf into bound and radiation contributions. It constituted an important rise of the credibility of the results reported in this work in comparison with the previous zero-crossing method since the whole time interval of the detectable signal was used for the data processing instead of some specific points on the time scale interval (so-called zero-crossing point[3]).

The empirical information on the position of bound contributions on the time scale obtained as a function of R provided the knowledge of correspondent time shifts related to propagation (causal) characteristics of bound em fields. According to standard views, if both positions are separated by a step ΔR then the speed of light c determines an observable time shift $\Delta t = \Delta R/c$. Nevertheless, experimentally found causal behavior of bound components in coaxial configurations showed no retardation ($\Delta t = 0$) inside the near zone, tending to the value $\Delta t = \Delta R/c$ at large distances.

As a cross verification of the results obtained in coaxial configuration, we carried out a comparison between numerically synthesized and recorded signals in coplanar configuration. Importantly, this analysis confirms that in coplanar configuration R^{-2} term [proportional to the factor $c/v(R)$] turns out to be strongly suppressed within the near zone where $v(R)$ is much greater than c. It ought to be considered as an additional argument in favor of the developed model used in coplanar configuration since it is based on the observable amplitude relations between different signals' components.

On a qualitative level, these data keep in line with the result of our previous work[3] and come to a fundamental disagreement with the current causal interpretation of the classical em theory. Put in other terms, within the near zone $R < \lambda/2\pi$ there is no empirical support for the validity of standard views with respect to the propagation of bound em fields with the speed of light. Specifically, gauge-independent bound fields alone exhibit nonlocal properties in the region of space close to em source where they are dominant. Strictly speaking, this result has to be distinguished from an *apparent superluminality* which takes place in the causal framework of the conventional em theory: phase velocities of the signal front as a superposition of bound and radiation components (propagating with the same rate) are *apparently greater than c* in the near zone.[6] This circum-

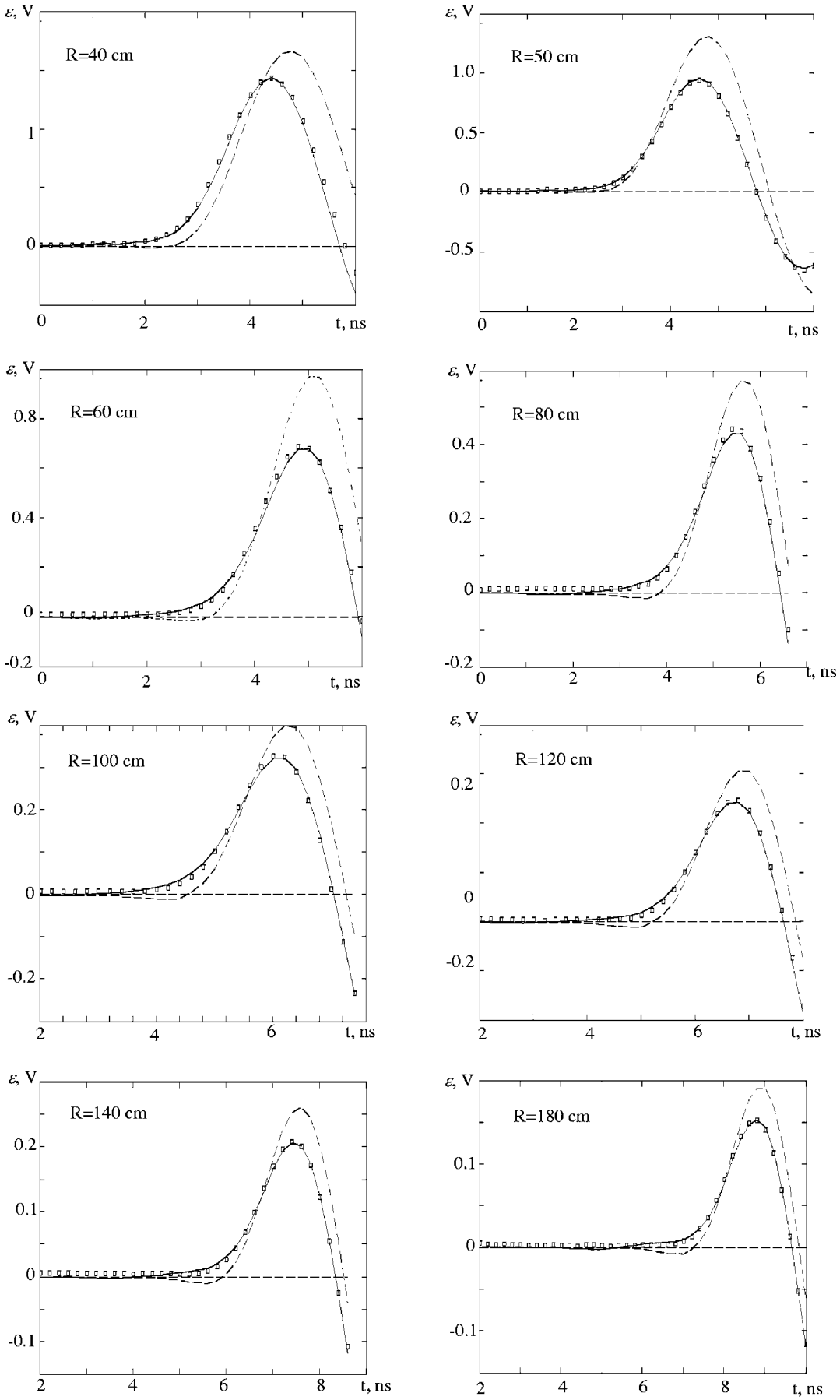

FIG. 7. Coplanar configuration: comparison of the detectable signal (hollow squares) produced in the RA at different spatial positions and numerically synthesized signals obtained under (a) the first hypothesis in agreement with the standard condition $v=c$ (dash lines) and (b) the second hypothesis with the causal framework of bound contributions determined by Eq. (18) (continuous lines).

stance highlights the importance to study the causal propagation of bound and radiation fields separately by the decomposition of the detectable signal into respective contributions.

At the present stage it is unrealistic and unreasonable to believe that the results reported in this work are sufficient to determine the causal framework meaningful for bound em fields at all length scales. There is an obvious need for complementary cross verifications based on independent methodological and experimental procedures. For instance, one might want to intend it by variation of intrinsic parameters such as the wavelength of em radiation which formally defines the frontier $\lambda/2\pi$ between the near and far zones. As a consequence, enhancing or reducing em radiation frequency will provide quantitative information on the causal propagation of em bound fields in smaller or in larger near zone, respectively.

The above-mentioned modifications of antenna's parameters represent nontrivial experimental task and might form part of complementary and independent investigations. In fact, any rise of the radiation frequency will require a proportional widening of the bandwidth of signal's recording setup. In the case of a smaller frequency a correspondent wavelength enlargement implies an extension of all laboratory dimensions: (a) length—to allow space for bigger distance variation and (b) width and height—to avoid reflections from walls, floor, and ceiling within a larger time interval. Therefore, such modifications will require substantial resources. It partly explains our opting for the same experimental setup (as used already in our previous work[3]) with all parameters carefully chosen and optimized for a particular laboratory room and equipment. Some of experimental tasks can be attributed to a more detailed investigation inside the region of space very close to em source, i.e., at $R \ll \lambda/2\pi$. It will require the elaboration of a more precise theoretical description useful at very small distances as well as a considerable effort in improving the timing resolution of our experimental measurements. Examination of these attempts will more likely constitute our next work.

From a foundational standpoint the manifested nonlocality of bound fields in regions close to em sources might suggest a previously unknown intimate relationship between classical bound em fields and quantum mechanical phenomena. Finally, we are tempted to think that these nonlocal properties exhibited by bound fields in the near zone are in agreement with Maxwell's fundamental equations and can be part of the paradigm of a causal physical theory which unifies classical and quantum descriptions. Another strong motivation for studying bound em fields realistically appears to be a perspective of possible implications for such important areas of applied physics as near fields of radiative systems, plasma physics, thermonuclear fusion, etc.

ACKNOWLEDGMENTS

Travel expenses were partly supported by BSCH/UCM 27/05-13939 and CM-910143. The authors also thank J. A. Santamaria Rueda (Moscow, Russia) for the crucial help in the realization of this project.

APPENDIX A: ACCOUNT FOR RETARDATION EFFECTS IN DERIVATION OF EMF

We start with (4) and following Ref. 3, we choose the distance R between the centers of EA and RA as the reference distance for the account of retardation effects attached to the standard retardation time $t-R/c$, where t is the present instant of time. Then, under the quasistationary current approximation, the value of conduction current I had the same value over the perimeter of EA at the retarded time $t-R/c$. Signals from different segments of EA will arrive at some observation point inside RA with different retarded times $t-R'/c$ (see Fig. 1). If $R' \neq R$, it corresponds to an additional time shift $\Delta t=(R'-R)/c$ with respect to the reference retarded time $t-R/c$. Nevertheless, if one knows the time variation of the conduction current $I(t)$, both values are easily interrelated by neglecting all second order retardation terms with respect to the difference $(R'-R)/c$,

$$I(t^{R'}) = I\left(t^R - \frac{R'-R}{c}\right) \cong (I)_c - \frac{R'-R}{c}\left(\frac{\partial I}{\partial t}\right)_c, \tag{A1}$$

where $t^{R'}=t-(R'/c)$ and $t^R=t-(R/c)$ are retarded times that correspond to the distances R' and R, respectively; $[I]_c$ and $(\partial I/\partial t)_c$ are being evaluated at t^R.

The same way of reasoning is also applicable to obtain an equivalent representation of $\partial I/\partial t$ and $\partial^2 I/\partial t^2$ generated at $t^{R'}$,

$$\frac{\partial I}{\partial t}(t^{R'}) = \frac{\partial I}{\partial t}\left(t^R - \frac{R'-R}{c}\right) \cong \left(\frac{\partial I}{\partial t}\right)_c - \frac{R'-R}{c}\left(\frac{\partial^2 I}{\partial t^2}\right)_c, \tag{A2}$$

$$\frac{\partial^2 I}{\partial t^2}(t^{R'}) = \frac{\partial^2 I}{\partial t^2}\left(t^R - \frac{R'-R}{c}\right) \cong \left(\frac{\partial^2 I}{\partial t^2}\right)_c - \frac{R'-R}{c}\left(\frac{\partial^3 I}{\partial t^3}\right)_c, \tag{A3}$$

where $(\partial I/\partial t)_c$, $(\partial^2 I/\partial t^2)_c$, and $(\partial^3 I/\partial t^3)_c$ are also determined at the reference retarded time $t^R=t-R/c$.

Using relations (A1)–(A3), expression (4) takes the most explicit form convenient for further calculations,

$$\varepsilon = \frac{r_{EA}^2}{4\pi\varepsilon_0 c^2}\int_0^{r_{RA}}\int_0^{2\pi}\int_0^{2\pi}\left\{\frac{(\partial I/\partial t)_c - [(R'-R)/c](\partial^2 I/\partial t^2)_c}{R'^3} + \frac{(\partial^2 I/\partial t^2)_c - [(R'-R)/c](\partial^3 I/\partial t^3)_c}{cR'^2}\right\}\xi r dr d\theta d\varphi. \tag{A4}$$

Reordering terms we obtain

$$\varepsilon = \frac{r_{EA}^2}{4\pi\varepsilon_0 c^2}\int_0^{r_{RA}}\int_0^{2\pi}\int_0^{2\pi}\left[\frac{(\partial I/\partial t)_c}{R'^3} + \frac{R'-R}{c}\frac{(\partial^2 I/\partial t^2)_c}{R'^3}\right]\times \xi r dr d\theta d\varphi + \frac{r_{EA}^2}{4\pi\varepsilon_0 c^2}\int_0^{r_{RA}}\int_0^{2\pi}\int_0^{2\pi}\left\{\frac{R}{c}\frac{(\partial^2 I/\partial t^2)_c}{cR'^2} - \frac{R'-R}{c}\frac{(\partial^3 I/\partial t^3)_c}{cR'}\right\}\xi r dr d\theta d\varphi. \tag{A5}$$

Additionally, in our quasistationary current approximation the present-time value of the conduction current I as

well as higher order time derivatives $\partial I/\partial t$, $\partial^2 I/\partial t^2$, etc., are not functions of φ in all segments of the EA. As a result, one can factor $\partial I/\partial t$, $\partial^2 I/\partial t^2$, etc., out from the integral sign so that Eq. (A5) can be given a compact form

$$\varepsilon = -\frac{S_{\mathrm{EA}}S_{\mathrm{RA}}}{4\pi\varepsilon_0 c^2}\left[k_{b1}\frac{(\partial I/\partial t)_c}{R^3} + k_{b2}\frac{(\partial^2 I/\partial t^2)_c}{cR^2} + k_{f1}\frac{(\partial^2 I/\partial t^2)_c}{cR^2} + k_{f2}\frac{(\partial^3 I/\partial t^3)_c}{c^2 R}\right], \tag{A6}$$

where

$$k_{b1} = \frac{R^3}{\pi^2 r_{\mathrm{RA}}^2}\int_0^{r_{\mathrm{RA}}}\int_0^{2\pi}\int_0^{2\pi}\frac{\xi}{R'^3}rdrd\theta d\varphi, \tag{A7}$$

$$k_{b2} = \frac{R^2}{\pi^2 r_{\mathrm{RA}}^2}\int_0^{r_{\mathrm{RA}}}\int_0^{2\pi}\int_0^{2\pi}(R-R')\frac{\xi}{R'^3}rdrd\theta d\varphi, \tag{A8}$$

$$k_{f1} = \frac{R^2}{\pi^2 r_{\mathrm{RA}}^2}\int_0^{r_{\mathrm{RA}}}\int_0^{2\pi}\int_0^{2\pi}\frac{\xi}{R'^2}rdrd\theta d\varphi, \tag{A9}$$

$$k_{f2} = -\frac{R}{\pi^2 r_{\mathrm{RA}}^2}\int_0^{r_{\mathrm{RA}}}\int_0^{2\pi}\int_0^{2\pi}(R-R')\frac{\xi}{R'^2}rdrd\theta d\varphi. \tag{A10}$$

In our numerical evaluations instead of Eq. (A5) we used a more advanced expression which takes into consideration also antenna width,

$$\varepsilon = \frac{r_{\mathrm{EA}}^2}{4\pi\varepsilon_0 c^2}\int_0^{h_{\mathrm{RA}}}\int_0^{r_{\mathrm{RA}}}\int_0^{2\pi}\int_0^{2\pi}\left\{\frac{(\partial I/\partial t)_c - [(R'-R)/c](\partial^2 I/\partial t^2)_c}{R'^3}\right\}\xi rdrd\theta d\varphi dh + \frac{r_{\mathrm{EA}}^2}{4\pi\varepsilon_0 c^2}\int_0^{h_{\mathrm{RA}}}\int_0^{r_{\mathrm{RA}}}\int_0^{2\pi}\int_0^{2\pi}\left\{\frac{(\partial^2 I/\partial t^2)_c - [(R'-R)/c](\partial^3 I/\partial t^3)_c}{cR'^2}\right\}\xi rdrd\theta d\varphi dh, \tag{A11}$$

where h_{RA} is the width of RA, R is now the distance between the centers of EA and RA placed in the intermediate position inside the antenna width, and all corresponding values R' and ξ are to be redefined to take into account new geometrical parameters h_{EA} and h_{RA}.

APPENDIX B: DECOMPOSITION OF RECORDED SIGNALS INTO BOUND AND RADIATION CONTRIBUTIONS IN COAXIAL CONFIGURATION

The purpose is to find the best possible correspondence between experimental data and theoretical model described by Eq. (19), so we first present it as

$$\varepsilon(R,t) = \frac{(\partial I/\partial t)_v}{R^3} + \frac{(\partial^2 I/\partial t^2)_c}{R^2} = \varepsilon_b(R,t) + \varepsilon_f(R,t), \tag{B1}$$

where $\varepsilon(R,t)$ stands for the recorded signal, $\varepsilon_b(R,t)$ and $\varepsilon_f(R,t)$ are bound and radiation contributions, respectively, and t is the present instant of time.

em signals detected at different distances R_1 and R_2 are related by a certain time shift and rescaling factor,

$$\varepsilon_f(R_1,t_1) = \left(\frac{R_2}{R_1}\right)^2\varepsilon_f\left(R_2, t_2 - \frac{R_2-R_1}{c}\right) \tag{B2}$$

in the case of radiation components and

$$\varepsilon_b(R_1,t_1) = \left(\frac{R_2}{R_1}\right)^3\varepsilon_b\left(t_2 - \frac{R_2-R_1}{\tilde{v}}\right) \tag{B3}$$

in the case of bound fields, where $\tilde{v}$ denotes an average velocity of bound magnetic fields in the space region $R_1 < R < R_2$.

At large distances the radiation component predominates and constitutes nearly the whole signal at $R_{\max}=300$ cm so that as a first approximation we can take

$$\varepsilon_f^{(1)}(R_{\max},t) = \varepsilon(R_{\max},t), \tag{B4}$$

where the superindex denotes the current number of iteration step.

As a result, using Eq. (B2) and rescaling $\varepsilon_f^{(1)}(R_{\max},t)$ with the factor $(R_{\max}/R)^2$, we are in a position to find a first approximation to the radiation contribution into emf at space positions $R=20-240$ cm,

$$\varepsilon_f^{(1)}(R,t) = \left(\frac{R_{\max}}{R}\right)^2\varepsilon_f^{(1)}\left(R_{\max}, t - \frac{R_{\max}-R}{c}\right), \tag{B5}$$

and the bound contribution by subtraction from the recorded signal,

$$\varepsilon_b^{(1)}(R,t) = \varepsilon(R,t) - \varepsilon_f^{(1)}(R,t). \tag{B6}$$

It constitutes one-step decomposition described in the main text (Sec. III A). In order to improve the precision of the decomposition procedure we shall first reconstruct the bound contribution at $R_{\min}$ where it has a maximum value,

$$\varepsilon_f^{(1)}(R_{\min},t) = \left(\frac{R_{\max}}{R_{\min}}\right)^2\varepsilon_f^{(1)}\left(R_{\max}, t - \frac{R_{\max}-R_{\min}}{c}\right), \tag{B7}$$

$$\varepsilon_b^{(1)}(R_{\min},t) = \varepsilon(R_{\min},t) - \varepsilon_f^{(1)}(R_{\min},t), \tag{B8}$$

then on the basis of Eq. (B3) we use $\varepsilon_b^{(1)}(R_{\min},t)$ in order to reconstruct $\varepsilon_b^{(1)}(R,t)$, at all intermediate positions within the

space region $R=30-240$ cm, and eventually we get the first approximation to the whole signal,

$$\varepsilon_{\mathrm{syn}}^{(1)}(R,t)=\varepsilon_b^{(1)}[R,t+\Delta t_b(R)]+\varepsilon_f^{(1)}(R,t), \tag{B9}$$

where $\varepsilon_f^{(1)}(R,t)$ is determined by (B5) and $\Delta t_b(R)$ describes the retardation of bound contribution as a function of R.

The bound contribution is now recovered not by a simple subtraction of $\varepsilon_f^{(1)}$ from the recorded signal ε but by direct rescaling of the bound contribution obtained at $R_{\min}$. Moreover, there is a free fitting parameter $\Delta t_b(R)$ in order to get the best correspondence with the recorded signal at each R within the domain of 30–240 cm.

For quantitative comparison between the synthesized and recorded signals, we introduce the error functional $\delta[R,\Delta t_b(R)]$ which gives a measure of the deviation between both signals,

$$\delta^{(1)}[R,\Delta t_b(R)]=\frac{100\%}{A(m_2-m_1)}\sqrt{\sum_{i=m_1}^{m_2}[\varepsilon(R,t_{Ri})-\varepsilon_{\mathrm{syn}}^{(1)}(R,t_{Ri})]^2}, \tag{B10}$$

where $\varepsilon(R,t_{Ri})$ and $\varepsilon_{\mathrm{syn}}^{(1)}(R,t_{Ri})$ are the recorded and synthesized signals in ith channel on the time scale of the digital oscilloscope, respectively, A is the amplitude of the recorded signal at the first half-period, and m_1 and m_2 determine the initial and the final channels of the signal half-period, respectively.

According to the definition, the functional (B10) characterizes an average deviation between the recorded and synthesized signals per channel. Varying the free fitting parameter $\Delta t_b(R)$ we find certain values $\Delta t_b^{(1)}(R)$ that lead to the minimization of the error functional $\delta^{(1)}[R,\Delta t_b^{(1)}(R)]$. It provides us with the first approximation to the positions of bound contributions at each R related explicitly to the retardation $\Delta t_b^{(1)}(R)$.

Now we are in a position to evaluate the bound contribution as a part of the recorded signal at the distance $R_{\max}$ where we earlier assumed the approximation (B4). Subtracting $\varepsilon_b^{(1)}(R_{\max},t)$ from the original recorded signal $\varepsilon(R_{\max},t)$, we get a better approximation to the radiation contribution at $R_{\max}$. We denote it as $\varepsilon_f^{(2)}(R_{\max},t)$ and repeat the iteration procedures [(B4)–(B9)]. Having made n running, we stop the procedure when the difference between $\delta^{(n)}[R,\Delta t_b^{(n)}(R)]$ and $\delta^{(n+1)}[R,\Delta t_b^{(n+1)}(R)]$ does not exceed 5% of $\delta^{(n)}$. Several runnings were sufficient to fulfill this requirement.

As an outcome of the described iteration procedure, we obtain the decomposition of the recorded signal into bound and radiation contributions at each R. The position of bound contributions obtained as a function of R is equivalent to the knowledge of the dependence $\Delta t_b(R)$ so that we are in a position to evaluate the average propagation velocity of bound fields according to $\Delta t_b(R)=(R_2-R_1)/\bar{v}$. We took the closest positions R_1 and R_2 available in experimental measurements in order to get the value of $\bar{v}[(R_2+R_1)/2]$.

[1]H. Hertz, in *Electric Waves, Collection of Scientific Papers* (Dover, New York, 1962).
[2]R. Smirnov-Rueda, Found. Phys. **35**, 1 (2005).
[3]A. L. Kholmetskii, O. V. Missevitch, R. Smirnov-Rueda, R. Ivanov, and A. E. Chubykalo, J. Appl. Phys. **101**, 023532 (2007).
[4]J. D. Jackson, *Classical Electrodynamics*, 2nd ed. (Wiley, New York, 1975).
[5]L. D. Landau and E. M. Lifshitz, *The Classical Theory of Fields* (Addison-Wesley, Cambridge, MA, 1951).
[6]W. K. H. Panofsky and M. Phillips, *Classical Electricity and Magnetism*, 3rd ed. (Addison-Wesley, Reading, MA, 1969), p. 260.
[7]W. G. V. Rosser, *Interpretation of Classical Electromagnetism*, Fundamental Theories of Physics Vol. 78, edited by A. Van der Merwe (Kluwer, Dordrecht, 1997).
[8]O. L. Brill and B. Goodman, Am. J. Phys. **35**, 832 (2005).
[9]J. D. Jackson and L. B. Okun, Rev. Mod. Phys. **73**, 663 (2001).
[10]F. Rohrlich, Am. J. Phys. **70**, 411 (2002).
[11]O. D. Jefimenko, *Electricity and Magnetism: An Introduction to the Theory of Electric and Magnetic Fields*, 2nd ed. (Electret Scientific, Star City, WV, 1989).
[12]J. A. Stratton, *Electromagnetic Theory* (McGraw-Hill, New York, 1941).